Available online at www.sciencedirect.com
ScienceDirect
International Journal of Heat and Mass Transfer 51 (2008) 2267–2281
International Journal of HEAT and MASS TRANSFER
www.elsevier.com/locate/ijhmt

Effects of inlet/outlet configurations on flow boiling instability in parallel microchannels

Guodong Wang [a], Ping Cheng [a,*], A.E. Bergles [b]

[a] School of Mechanical and Power Engineering, Shanghai Jiaotong University, Shanghai 200240, PR China
[b] Mechanical Engineering Department, Massachusetts Institute of Technology, Cambridge, MA 02139, United States

Received 21 May 2007; received in revised form 15 August 2007
Available online 29 October 2007

Abstract

A simultaneous visualization and measurement study has been carried out to investigate effects of inlet/outlet configurations on flow boiling instabilities in parallel microchannels, having a length of 30 mm and a hydraulic diameter of 186 μm. Three types of inlet/outlet configurations were investigated. Fluid flow entering to and exiting from the microchannels with the Type-A connection was restricted because the inlet and outlet conduits were perpendicular to the microchannels. The fluid flow had no restriction in entering to and existing from the microchannels with the Type-B connection. In the Type-C connection, fluid flow was restricted in entering each microchannel but was not restricted in exiting from the microchannels. It is found that amplitudes of temperature and pressure oscillations in the Type-B connection are much smaller than those in the Type-A connection under the same heat flux and mass flux conditions. On the other hand, nearly steady flow boiling exists in the parallel microchannels with the Type-C connection under the experimental conditions. Therefore, this configuration is recommended for high-heat-flux microchannel applications. As predicted, the stability threshold is determined by the minimum in the pressure-drop-versus-flow-rate curve. The pressure drop and heat transfer coefficient versus vapor quality for flow boiling in microchannels with the Type-C connection are presented. It is found that experimental data of pressure drop are higher and heat transfer coefficients are lower for boiling flow at high vapor quality in microchannels than those predicted from correlation equations for boiling flow in macrochannels, due to local dryout.

Keywords: Boiling instability; Microchannels; Reversed flow; Inlet restriction

1. Introduction

Boiling instabilities in a single macrochannel have been a topic of extensive study since the mid 1960s. Boure et al. [1] identified the causes and mechanisms of flow boiling instability modes, and suggested that two-phase flow instabilities in a single macrochannel could be divided into dynamic and static categories. The former includes the pressure drop oscillation that is caused by upstream compressible volume instability while the latter includes flow excursive instability. As discussed by Daleas and Bergles [2], any upstream compressibility can affect the local heat transfer characteristics and may introduce boiling crisis (critical heat flux) that causes mechanical damage [3].

In recent years, two-phase flow instabilities in microchannels have attracted considerable attention [4–23]. Brutin et al. [6] investigated two-phase instabilities in a microchannel with a hydraulic diameter of 889 μm, and a flow map in terms heat flux versus mass flux was presented for steady and unsteady two-phase flows. Hetsroni et al. [7,8] found small pressure fluctuations in flow boiling of water in 21 silicon triangular microchannels having a diameter of 129 μm, and observed periodic annular flow and dry steam flow in these microchannels. Wu and Cheng [9,10] carried out a simultaneous visualization and measurement investigation on flow boiling of water in parallel silicon microchannels of trapezoidal cross-section having

* Corresponding author. Tel.: +86 02134200337; fax: +86 02134206337.
E-mail address: pingcheng@sjtu.edu.cn (P. Cheng).

0017-9310/$ - see front matter © 2007 Elsevier Ltd. All rights reserved.
doi:10.1016/j.ijheatmasstransfer.2007.08.027

Nomenclature

A_c	cross-sectional flow area of each microchannel (m^2)
A_w	area of microchannel bottom wall and side walls of each channel (m^2)
G	mass flux ($kg\,m^{-2}\,s^{-1}$)
h_e	exit fluid enthalpy ($J\,kg^{-1}$)
h_{in}	inlet fluid enthalpy ($J\,kg^{-1}$)
h_f	saturated liquid enthalpy ($J\,kg^{-1}$)
h_{fg}	latent heat of evaporation ($J\,kg^{-1}$)
h_{local}	local heat transfer coefficient at exit ($W\,m^{-2}\,K^{-1}$)
I	electric current of heater (A)
k	thermal conductivity of silicon substrate ($W\,m^{-1}\,K^{-1}$)
L	total heating length (m)
N	total number of microchannels
q	heat flux ($W\,m^{-2}$)
V	electric voltage of heater (V)
ΔP	pressure drop (bar)
t	time (s)
T	temperature (°C)
t_b	distance from the heat sink base to the bottom of the microchannel (m)
x_e	thermodynamic vapor quality (–)

Greek symbol

Φ	heat transfer ratio

Subscripts

b	bottom of microchannel substrate
c	contraction
e	expansion
in	inlet
exp	experimental
out	outlet
pred	predicted
re	restriction
sp	single phase
tp	two phase
w	wall

hydraulic diameters of 82.8 μm, 158.8 μm, and 185.6 μm. They found that there existed two oscillatory flow boiling modes with large amplitudes of temperature and pressure fluctuations in microchannels: liquid/two-phase alternating flow and liquid/two-phase/vapor alternating flow. Subsequently, Hetsroni et al. [11] observed the explosive boiling phenomena with periodic wetting and dryout in flow boiling in triangular silicon parallel microchannels. Xu et al. [12] conducted experiments to study transient flow boiling pattern of acetone in 10 triangular microchannels with a hydraulic diameter of 155.4 μm, and found that the heat transfer coefficient depended on the boiling number. Most recently, Wang et al. [13] performed further experimental studies on flow boiling in parallel microchannels and in a single microchannel, and found there were three flow boiling modes, depending on the heat-to-mass-flux ratio, q/G and the inlet water temperature. A comparison of temperature fluctuations in flow boiling in parallel microchannels and in a single microchannel shows that flow interaction effects from neighboring channels at the headers of the parallel microchannels are significant. Two boiling flow pattern maps in terms of heat flux versus mass flux, showing the three flow boiling modes at a specific inlet water temperature, were presented for parallel microchannels and a single microchannel. The large amplitude fluctuations of pressure and temperature in unstable flow boiling modes can be attributed to the backward expansion of vapor bubbles in these microchannels owing to the confined space [11,13].

Qu and Mudawar [14] performed a flow boiling experiment of water in a heat sink made of 21 copper parallel microchannels with a cross-section area of $231 \times 713\ \mu m^2$. They installed a throttle valve in the inlet line before the header, and found that the severe pressure drop oscillation due to compressible volume instability was virtually eliminated, but small fluctuations, termed "parallel channel interactions", remained. Kandlikar et al. [15] used inlet area restriction (96%) to each channel and artificial nucleation sites to suppress the instabilities during flow boiling in a set of six $1054 \times 197\ \mu m^2$ parallel channels. They found that this configuration completely eliminated the instabilities. Bergles and Kandlikar [17] earlier suggested that inlet orifices be fabricated at each microchannel to suppress both the excursive instability and the compressible volume instability. Kosar et al. [19] investigated geometrical effects of inlet orifices in each microchannel to suppress boiling flow instabilities, and used a pressure drop multiplier to correlate the extent of flow oscillation suppression.

In this paper, we have performed further simultaneous visualization and measurement study to investigate the effects of inlet/outlet configurations on dynamic instabilities in flow boiling of water in microchannels, having a hydraulic diameter of 186 μm that were used in our previous work [9,10,13]. Flow boiling instabilities in parallel microchannels with three types of connections were compared. In the Type-A connection, inlet and outlet conduits were perpendicular to the parallel microchannels in the test section. In the Type-B connection, fluid could flow into and exit from the parallel microchannels without any restriction, and in the Type-C connection, fluid entered each of the microchannels through an inlet restriction. Measurements of wall temperatures, inlet/outlet water temperatures, and inlet/outlet pressures, were recorded. In

addition, with the aid of a microscope and a high-speed video recording system, typical flow boiling patterns in microchannels with Type-B and Type-C connections were observed. Pressure drop and heat transfer coefficient versus exit vapor quality in flow boiling in microchannels with the Type-C connection are presented.

2. Description of the experiment

2.1. Experimental setup

Fig. 1 shows the test facility and flow circuit used in the present experiment. The deionized and degassed water in the high-pressure tank, being pushed by the compressed nitrogen gas, flowed successively through a ball valve, a degassing unit (to remove the dissolved gas), a constant temperature bath (to ensure a certain inlet water temperature), a 0.5 μm-filter, a needle valve (to regulate the mass flux) and finally the heated microchannel block. The steam discharged from the microchannels was collected in a container, which had a small hole vented to the atmosphere. The container was placed on a precision electronic balance, and the average mass flux of water was determined by calculating the mass increment per unit time. It is relevant to point out that the needle valve was placed behind the filter in the present experiment, which differed from those of our previous experiments [9,10,13] in which the needle valve was placed ahead of the filter.

2.2. Test section

The eight parallel microchannels, having the same length and identical trapezoidal cross-sectional area and etched in a ⟨100⟩ silicon substrate, are shown in Fig. 2.

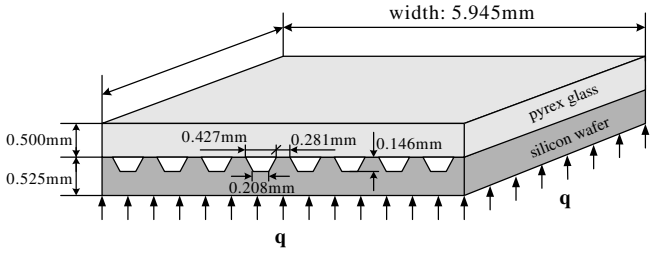

Fig. 2. Arrangement of parallel microchannels on silicon wafer.

The top width, bottom width, and depth of these trapezoidal microchannels were 427 μm, 208 μm, and 146 μm, respectively. These microchannels, having a hydraulic diameter of 186 μm and a length of 30 mm, were the same as those used in our previous work [9,10,13]. The distance between two neighboring microchannels was 281 μm. The microchannels were sealed from the top by a thin Pyrex glass plate, which allowed visualization of boiling phenomena.

2.3. Inlet/outlet configurations

Fig. 3 is a schematic representation of three types of inlet/outlet connections with the parallel microchannels in the test section. Fig. 3(a) shows the Type-A connection in which water was supplied by one inlet conduit perpendicular to the microchannels and discharged through one outlet conduit perpendicular to the microchannels. This type of connection was used in our previous work [9,10,13], where fluid flow in both inlet and outlet plenums were restricted. It should be noted that the experimental setup used by Wu and Cheng [9,10] were similar to that of Wang et al. [13] except that the former used a soft rubber tube to connect the filter and the inlet of microchannels while the latter

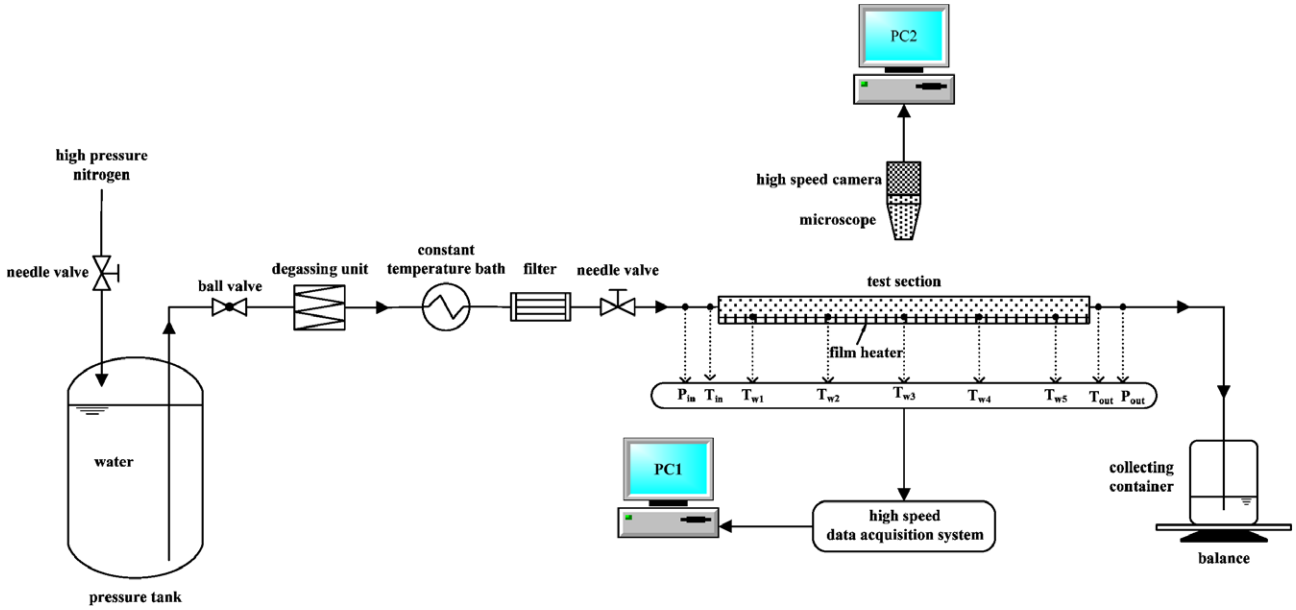

Fig. 1. Experimental test loop.

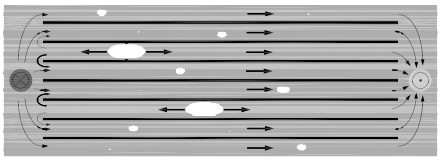

(a) Type-A connections: flow entering and exiting from parall microchannels with restrictions because inlet/outlet conduits perpendicular to microchannels

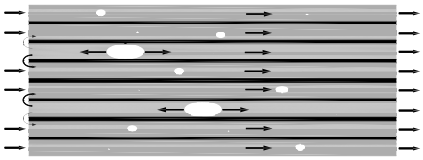

(b) Type-B connection: flow entering to and exiting from microchannels freely without restriction

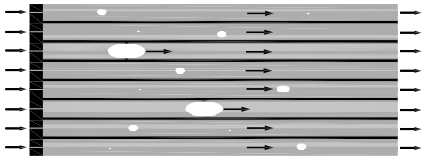

(i) Arrangement of parallel microchannels with restrictive inlet

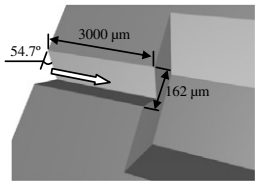

(ii) Sketch of the microchannel with a restrictive inlet

(c) Type-C connection: flow entering with restriction and exiting without restriction in microchannels

Fig. 3. Parallel microchannels with three different inlet/outlet connections.

used a stiff plastic tube to connect the filter and the inlet of microchannels. The larger compressible upstream volume in Wu and Cheng's experiments [9,10] caused larger amplitude (from 100 °C to 340 °C) and longer period (about 53 s) of temperature oscillations than that obtained by Wang et al. [13]. Fig. 3(b) shows the Type-B connection where the fluid was free to flow into and out of the microchannels, which was the configuration used by most of other investigators [7,8,11,12,14,20].

Fig. 3(c)(i) shows the Type-C connection where fluid flow entered each microchannel through a restrictive inlet while fluid flow could freely discharge from the outlet. This type of connection was suggested by Bergles [16] and Bergles and Kandlikar [17], which was used by Kandlikar et al. [15] and Kosar et al. [19] in their experiments on flow boiling in microchannels. Fig. 3(c)(ii) shows the cross-section of each inlet restriction in the Type-C connection, which was an isosceles triangle with a base of 162 μm whose two angles were 54.7°. The inlet restriction had a length of 3 mm, and its cross-sectional area was about 20% of that of the microchannels.

2.4. Measurement system

The test section, used in our previous work [9,10,13], was also used in this experiment. Therefore, the test section will only be briefly described here. As shown in Fig. 4, T_{b1}, T_{b2}, T_{b3}, T_{b4}, and T_{b5} were the temperatures at the bottom of microchannel substrate (about 379 μm below the bottom wall of the microchannels), and T_{in} and T_{out} were the fluid temperatures in the inlet and outlet of the microchannels. These temperatures were measured by seven type-T thermocouples, having a bead diameter of 0.1 mm with a response time of 0.1 s. Two pressure transducers with a response time of 0.001 s were used to measure water pressures (P_{in} and P_{out}) at inlet and outlet of the microchannels. All temperature and pressure signals were collected by a NI high-speed data acquisition system, and LabView

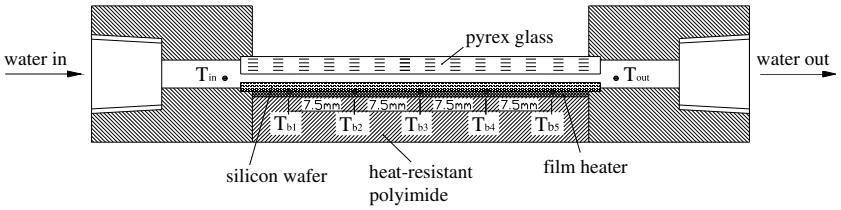

Fig. 4. Cross-sectional view of test section.

software was used to monitor the signals. A microscope was placed above the microchannels with a camera adapter to connect the microscope to a high-speed camera. The high-speed camera, with a maximum frame rate of 5145 fps at full resolution of 512 pixels × 512 pixels, was used to visualize flow boiling patterns in the microchannels.

2.5. Data reduction

The heat flux, q, is computed from $q = \Phi VI/A_w$, where V and I are the input voltage and current to the film heater, A_w the area of heated wall, and Φ the ratio of the heat absorbed by the working fluid to the total power input to the film heater. A series of single-phase heat transfer experiments were performed prior to the boiling heat transfer tests. The range of the heat transfer ratio, Φ, was determined and the mean heat transfer ratio of 0.89 was used to compute the effective heating power in the flow boiling experiment. The method was similar to those used by Hetsroni et al [7,8] and Xu et al. [12,22], which was also used in our previous work [9,10,13].

The average mass flux of water is given by $G = \Delta M/(\Delta t \cdot N \cdot A_c)$, where ΔM is the total mass increment in the container measured by an electronic balance during an appropriate time interval Δt (approximately 1 min); N is the total number of microchannels and A_c is the cross-sectional area of the microchannel. Thus, the mass flux reported in this paper was an average mass flux during Δt, and was not an instantaneous value.

The thermodynamic vapor quality at the exit, x_e, was computed according to

$$x_e = (h_e - h_f)/h_{fg} \tag{1}$$

where h_f is the saturated liquid enthalpy, h_{fg} is the latent heat of evaporation (both were evaluated at the exit pressure), and h_e is the fluid enthalpy at the exit, which can be calculated from

$$h_e = h_{in} + \frac{q \cdot N \cdot A_w}{G \cdot N \cdot A_c} \tag{2}$$

where h_{in} is the inlet fluid enthalpy, N is the total number of microchannels, A_w is the area of microchannel bottom wall and side walls of each channel, and A_c is the cross-sectional area of each microchannel. Substituting Eq. (2) into Eq. (1) gives the exit vapor quality:

$$x_e = \frac{h_e - h_f}{h_{fg}} = \frac{h_{in} + (A_w/A_c)q/G - h_f}{h_{fg}} = \frac{h_{in} - h_f}{h_{fg}} + \frac{A_w Bo}{A_c} \tag{3}$$

where $Bo = q/Gh_{fg}$ is the boiling number. The above equation shows that the value of x_e can be negative, zero, or positive depending whether the exit enthalpy h_e is less than, equal to, or greater than the saturated liquid enthalpy h_f. Eq. (3) also shows that the exit vapor quality x_e depends linearly with respect to q/G (or Bo) and also depends on the inlet water temperature and the geometry of the microchannel.

The local heat transfer coefficient at the exit, h_{local}, is computed from $h_{local} = q/(T_w - T_{out})$. The wall temperature T_w, is obtained by correcting the temperature measured at the bottom of the microchannel substrate, T_b, using $T_w = T_b - (q \cdot t_b)/k$, in which t_b is the distance from the heat sink base to the bottom of the microchannel, and k the thermal conductivity of silicon substrate.

3. Results and discussion

3.1. Flow boiling characteristics in microchannels with the Type-A connection

Flow boiling experiments in microchannels with the Type-A connection were carried out in the experimental setup shown in Fig. 1 under the same heat flux and mass flux conditions as those in Wang et al. [13]. Although the sequence of filter and valve in the present experimental setup was different from those used by Wang et al. [13], it was found that there were not much differences in temperature fluctuations measurements. This is probably owing to the fact that the 0.5 μm-filter and the needle valve acted as two valves in series that caused a large pressure drop but its sequence does not make any difference.

3.2. Flow boiling characteristics in microchannels with the Type-B connection

Experiments with the Type-B connection were carried out over a range of heat fluxes from $q = 184.2\ \mathrm{kW/m^2}$ to $485.5\ \mathrm{kW/m^2}$ with inlet water temperature at 35 °C. As mentioned previously, the fluid could enter and exit freely in the microchannels with the Type-B connection. Similar to our previous work with the Type-A connection [13], it was found that stable and unstable flow boiling regimes also existed in microchannels with the Type-B connection, depending on the heat to mass flux ratio, q/G (or Bo) and the inlet water temperature.

Fig. 5(a) and (b) are diabatic flow pattern maps, in terms of heat flux q versus mass flux G and heat flux q versus exit vapor quality x_e at an inlet water temperature of 35 °C (i.e., $T_{in} = 35$ °C), respectively. The inclined straight lines for $q/G = 1.01$ kJ/kg and for $q/G = 1.37$ kJ/kg at the inlet water temperature of 35 °C in Fig. 5(a) become vertical straight lines at $x_e = 0.044$ and $x_e = 0.103$ in Fig. 5(b) because x_e depends on both the value of q/G and inlet water temperature according to Eq. (3). These maps show that there are three different flow regimes with the Type-B connection: (i) steady flow boiling existed for $q/G < 1.01$ kJ/kg and $T_{in} = 35$ °C (i.e., $x_e < 0.044$), (ii) bubbly/annular alternating flow boiling existed for $1.01\ \mathrm{kJ/kg} < q/G < 1.37\ \mathrm{kJ/kg}$ and $T_{in} = 35$ °C (i.e., $0.044 < x_e < 0.103$), and (iii) annular/mist alternating flow boiling existed for $q/G > 1.37$ kJ/kg and $T_{in} = 35$ °C (i.e., $x_e > 0.103$). The unsteady flow boiling regime was due to the reversed flow of vapor

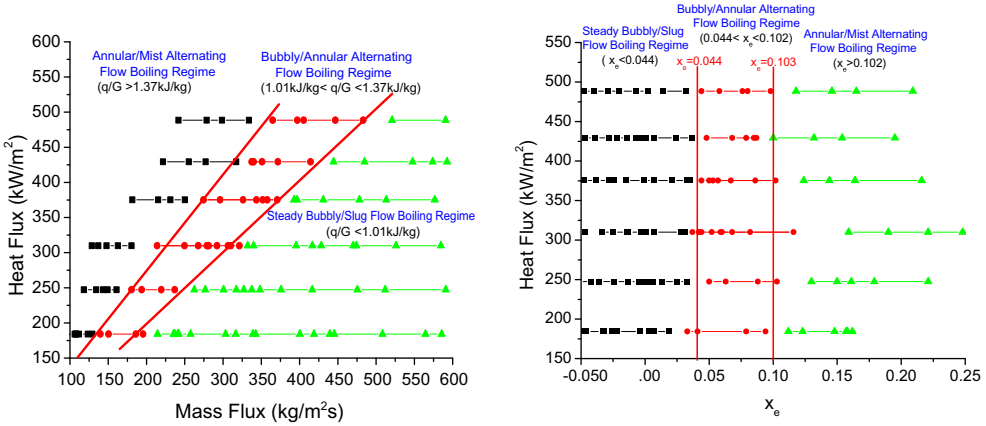

(a) Heat flux versus mass flux at T_{in} = 35 °C (b) Heat flux versus vapor quality at T_{in} = 35 °C

Fig. 5. Different flow boiling pattern in parallel microchannels (D_h = 186 μm) with the Type-B connection.

bubbles. Note that the steady bubbly/slug-flow regime in the Type-B connection with $q/G < 1.01$ kJ/kg and $T_{in} = 35$ °C ($x_e < 0.044$) in the present data is larger than that in the Type-A connection with $q/G < 0.96$ kJ/kg and $T_{in} = 35$ °C ($x_e < 0.036$) in our previous work [13]. This suggests that instability in parallel microchannels with the Type-B connection (where flow could exit freely from the microchannels) was partially reduced as compared with those with the Type-A connection where the flow could not exit freely because of the vertical outlet conduit.

3.2.1. Steady bubbly/slug flow boiling regime ($x_e < 0.044$)

Fig. 6(a) is a series of photos for the steady bubbly flow pattern with the Type-B connection at $q = 485.5$ kW/m^2 and $G = 787.3$ kg/m^2 s (i.e., $q/G = 0.617$ kJ/kg) and $T_{in} = 35$ °C ($x_e = -0.02$) for (i) near the entrance (T_{w1}), (ii) near the middle section (T_{w3}), and (iii) near the outlet section (T_{w5}). The photos were taken from the top of the microchannels through a transparent cover with a microscope lens of 50 magnifications at a frame rate of 22 300 fps. The bulk flow direction was from left to right. It can be seen from Fig. 6(a) that isolated bubbles grew near the entrance (i) and detached to move downstream. As the bubbles were flushed away, isolated bubbles formed a large bubble downstream due to bubbles coalescence and finally touched the heated walls or the top Pyrex glass cover as shown in (ii). Vapor plugs were formed near the outlet section (iii) as a result of the merging bubbles upstream. The steady bubbly/slug flow boiling patterns in the microchannels are sketched in Fig. 6(b).

Temporal variations of temperatures (including T_{in}, T_{out}, and T_{w1}–T_{w5}) and inlet/outlet pressures in the microchannels for the bubbly/slug flow in Fig. 6 are presented in Fig. 7(a) and (b), respectively. It is shown that all temperature and pressure measurements remained constant with time. The axial wall temperature (T_{w1}–T_{w5}) increased along the flow direction from the entrance (T_{w1}) to the outlet (T_{w5}). The outlet water temperature was about 89.8 °C while wall temperatures were at superheated conditions ranging from 104.9 °C to 121.6 °C.

3.2.2. Bubbly/annular alternating flow boiling regime ($0.044 < x_e < 0.103$)

For comparison purposes, flow boiling experiments in microchannels with the Type-B connection during the bubbly/annular alternating flow boiling regime were performed at a constant heat flux of $q = 485.5$ kW/m^2 and mass flux of $G = 364.9$ kg/m^2 s (i.e., $q/G = 1.33$ kJ/kg)

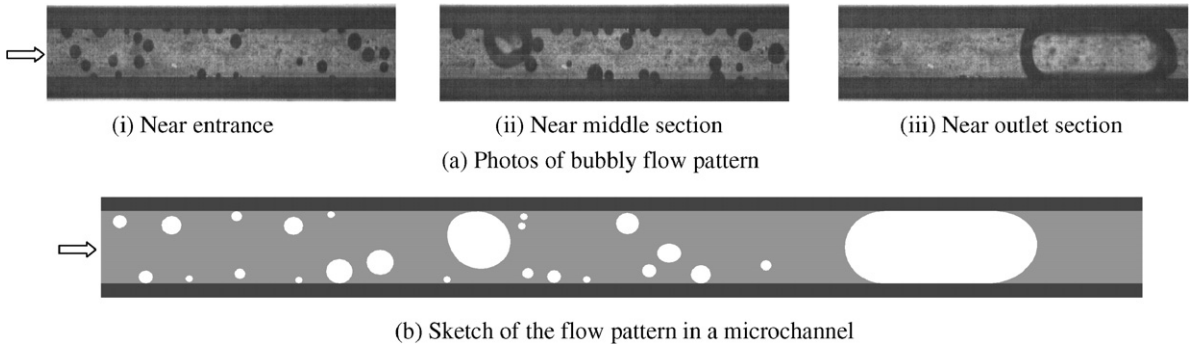

Fig. 6. Photos and sketch of flow patterns in steady bubbly/slug flow boiling regime in parallel microchannels (D_h = 186 μm) with the Type-B connection at $q = 485.5$ kW/m^2, $G = 787.3$ kg/m^2 s and $T_{in} = 35$ °C (i.e., $x_e = -0.02$).

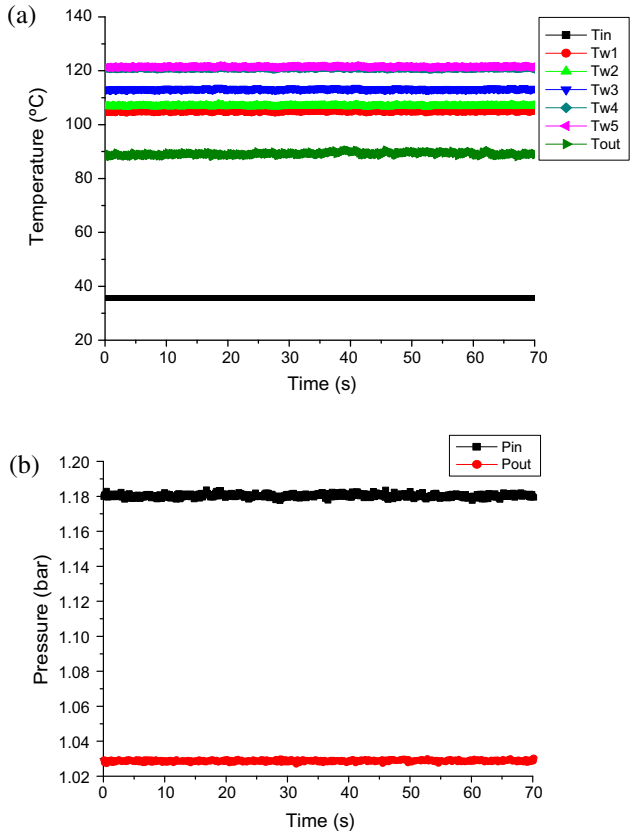

Fig. 7. Measurements of inlet/outlet water and wall temperatures and inlet/outlet pressures in parallel microchannels ($D_h = 186$ μm) with the Type-B connection at $q = 485.52$ kW/m^2, $G = 787.32$ kg/m^2 s and $T_{in} = 35$ °C (i.e., $x_e = -0.02$).

and $T_{in} = 35$ °C (or $x_e = 0.096$), where the heat flux and mass flux were approximately the same as those in the Type-A connection at $q = 497.8$ kW/m^2, $G = 368.9$ kg/m^2 s and $T_{in} = 35$ °C (or $x_e = 0.099$) in our previous work [13]. Fig. 8 presents a series of photos for one cycle of the bubbly/annular alternating flow patterns in the parallel microchannels with the Type-B connection under the aforementioned conditions. These photos were taken at a frame rate of 21 400 fps, and the bulk flow direction was from left to right. It can be seen from Fig. 8(a) that isolated bubbles were formed near the entrance surface of microchannels while confined bubbles were observed near the outlet section. At a later time, another bubble near the middle section (ii) in Fig. 8(b) grew to a larger size. After it had touched the heated walls, it began to expand rapidly in both upstream (i) and downstream (ii) directions, as shown in Fig. 8(c). This shows that reversed flow of vapor bubble also existed in microchannels with the Type-B connection where the flow can exit freely from the microchannels. An annular flow pattern was observed near the outlet section (iii) as shown in Fig. 8(c). When the inlet pressure was increased sufficiently to overcome the vapor bubble advancing upstream, incoming subcooled liquid rushed into the microchannels and the bubbly flow as shown in Fig. 8(a) occurred again, thus beginning a new cycle. While the reverse flow occurred in a channel, flow rates through adjacent channels were increased.

Fig. 9(a) shows measurements of inlet/outlet water temperatures, wall temperatures and inlet/outlet pressures in the microchannels with the Type-B connection for the same conditions shown in Fig. 8, whereas Fig. 9(b) shows the same measurements under similar conditions with the Type-A connection. A comparison of Fig. 9(a) and (b) shows that temperature and pressure oscillations in microchannels with the Type-B connection (Fig. 9a) were considerably less than those for the Type-A connection (Fig. 9b). It can be concluded that microchannels with the Type-B connection are more stable than those with the Type-A connection because the exit is more restrictive in the latter case.

3.2.3. Annular/mist alternating flow boiling regime ($x_e > 0.103$)

Fig. 10 presents the photos for annular/mist alternating flow patterns with the Type-B connection for one cycle at $q = 485.5$ kW/m^2, $G = 91.4$ kg/m^2 s and $T_{in} = 35$ °C ($x_e = 0.745$), which were taken at a frame rate of 21 400 frame/s. Near the entrance (i), a vapor bubble was formed and elongated (a)–(b), expanded both upstream causing an annular flow pattern (c), and disappeared in (d). Near the middle section (ii), the mist flow (a) changed to the churn flow (b)–(c), which was characterized by an intense mixing of the liquid and the vapor phase and then changed to mist flow (d). The alternating flow pattern between churn flow and mist flow near the middle section did not result in a sharp increase in the wall temperature due to the periodic wetting and rewetting process. Near the outlet section (iii), water droplets accumulated to rivulets on the bottom side of the top Pyrex glass as shown in (b)–(d). However, the local dryout on the wall near the outlet section did not lead to a sharp temperature increase because of high heat conduction in the silicon base until dryout occurred everywhere in the channels.

Pressure and temperature measurements for $q = 485.5$ kW/m^2 and $G = 91.4$ kg/m^2 s at $T_{in} = 35$ °C (or $x_e = 0.745$) with the Type-B connection (i.e., the case corresponding to Fig. 10) were also recorded. Fig. 11(a) shows inlet pressure fluctuations with a period of 0.03 s, which were measured by a pressure transducer with a response time of 0.001 s. For comparison purposes, pressure oscillations in parallel microchannels with the Type-A connection under similar condition are presented in Fig. 11(b). A comparison of Fig. 11(a) and (b) reveals that the oscillation amplitude for the Type-B was smaller than that for Type-A although the oscillation periods are almost the same. In addition, while periodic noises could be heard due to the violent collapse of the vapor plug in the inlet plenum with the Type-A connection, no periodic noises with the Type-B connection were heard probably because the backward expansion of the vapor bubble did not enter deep enough into the inlet plenum and no strong condensation took place at the vapor–liquid interface. Also, because of the relatively long response time of the type-T thermocou-

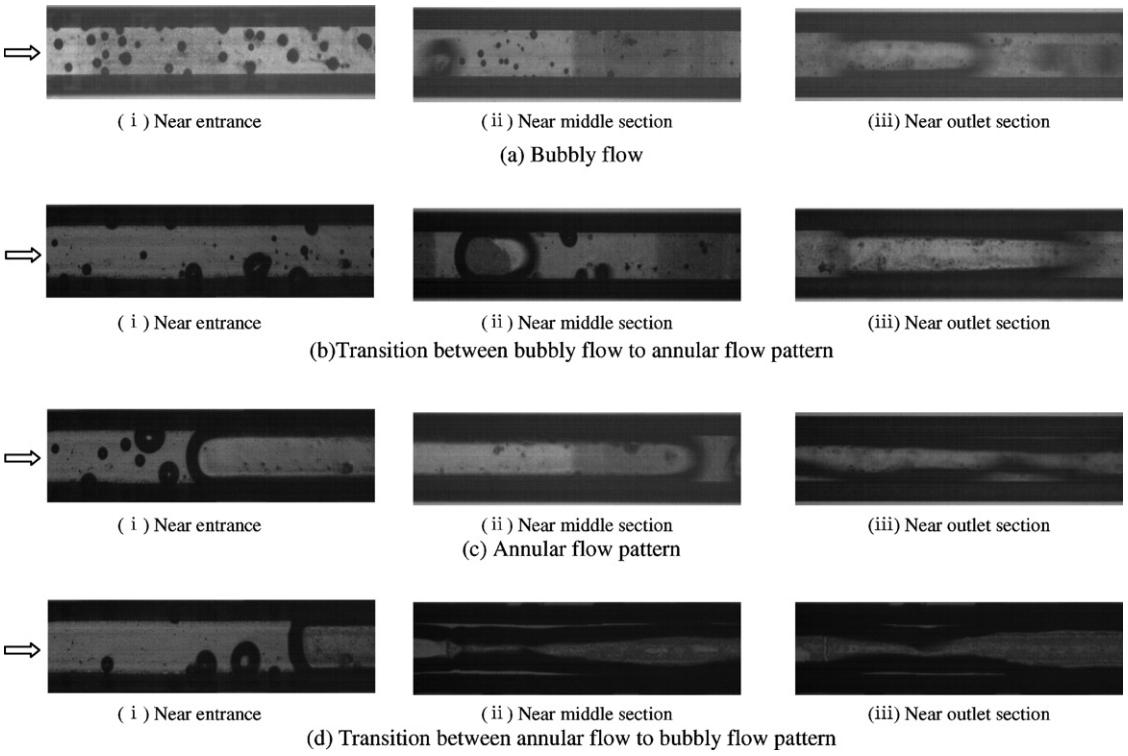

Fig. 8. Photos of flow patterns in one period from (a) to (d) in bubbly/annular flow boiling regime in parallel microchannels ($D_h = 186$ μm) with the Type-B connection at $q = 485.52$ kW/m^2, $G = 364.90$ kg/m^2 s and $T_{in} = 35$ °C (i.e., $x_e = 0.096$).

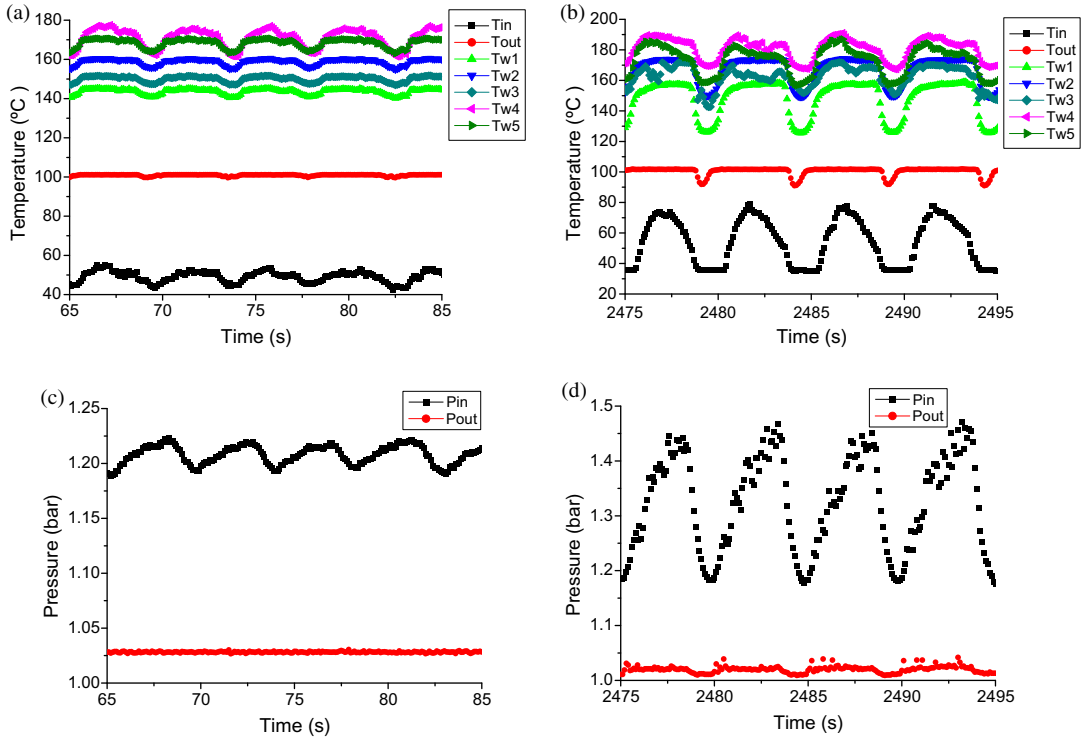

(a) Type-B with $x_e = 0.096$ and $T_{in} = 35$ °C (b) Type-A with $x_e = 0.099$ and $T_{in} = 35$ °C

Fig. 9. Measurements of inlet/outlet water and wall temperatures and inlet/outlet pressures in parallel microchannels ($D_h = 186$ μm) in bubby/annular alternating flow boiling regimes: (a) Type-B connection with $q = 485.52$ kW/m^2, $G = 364.90$ kg/m^2 s and $T_{in} = 35$ °C ($x_e = 0.096$) and (b) Type-A connections with $q = 497.80$ kW/m^2, $G = 368.94$ kg/m^2 s and $T_{in} = 35$ °C ($x_e = 0.099$).

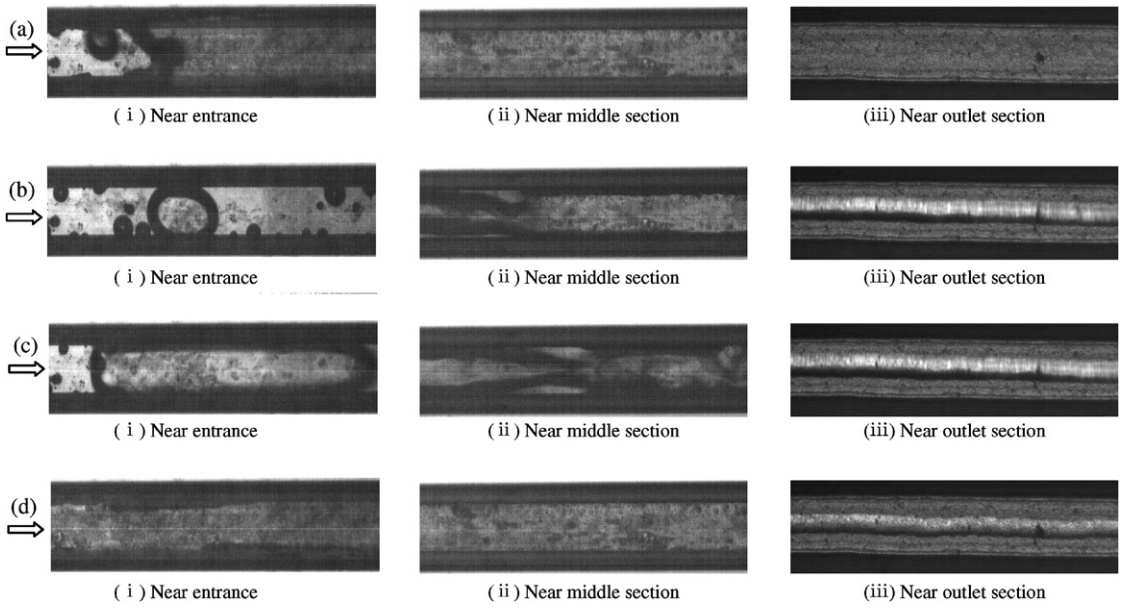

Fig. 10. Photos of flow patterns in one period from (a) to (d) in annular/mist flow boiling regime in parallel microchannels ($D_h = 186$ μm) with the Type-B connection at $q = 485.52$ kW/m^2, $G = 91.43$ kg/m^2 s ($q/G = 5.31$ kJ/kg) and $T_{in} = 35$ °C (or $x_e = 0.745$).

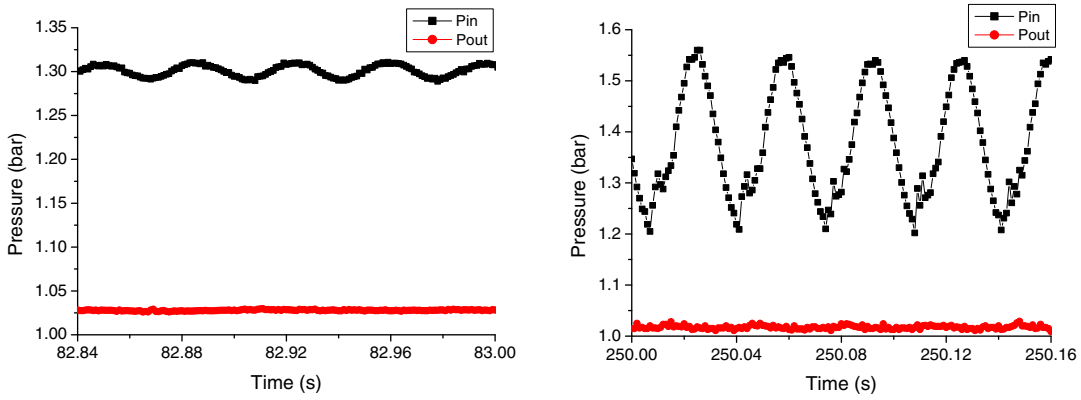

(a)Type-B connection with $x_e = 0.745$ and $T_{in} = 35$ °C (b)Type-A connection with $x_e = 0.762$ and $T_{in} = 35$ °C

Fig. 11. Measurements of inlet/outlet pressures in parallel microchannels ($D_h = 186$ μm) in annular/mist alternating flow boiling regime: (a) Type-B connection with $q = 485.52$ kW/m^2, $G = 91.43$ kg/m^2 s and $T_{in} = 35$ °C ($x_e = 0.745$) and (b) Type-A connection with $q = 484.70$ kW/m^2, $G = 89.53$ kg/m^2 s and $T_{in} = 35$ °C ($x_e = 0.762$).

ples (about 0.1 s), it was impossible to measure temperature oscillations.

It is interesting to note that the elongated bubbles in steady bubbly/slug flow were caused by bubbles coalescence at high mass fluxes (low x_e) as shown in Fig. 6, while the elongated bubbles in bubbly/annular and annular/mist alternating flow boiling were caused by rapid bubble expansion at low mass fluxes (high x_e) as shown in Figs. 8 and 10. The rapid expansion of the bubble upstream was the main source of oscillations noted in Fig. 5.

3.3. Flow boiling characteristics in microchannels with the Type-C connection

As mentioned earlier, Bergles et al. [16] and Bergles and Kandlikar [17] emphasized the necessity of installing inlet orifices in order to suppress both upstream compressible volume instability and excursive instability. Inlet orifices should also suppress the "parallel channel interactions" observed with both Type-A and Type-B connections. In the following, the investigation on flow boiling characteristics in parallel microchannels with the Type-C connection will be discussed, where such inlet restrictions had been fabricated.

3.3.1. Flow boiling patterns

Because the inlet restriction on each of the microchannels could prevent vapor babbles from expanding upstream, no reversed flow of vapor was observed in microchannels with the Type-C connection. Since all temperatures and pressures were constant with time, these data are not presented here.

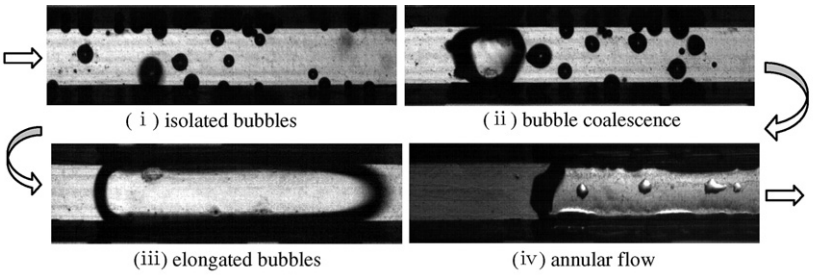

(a) Photos of steady flow boiling pattern in parallel microchannels with the Type-C connection

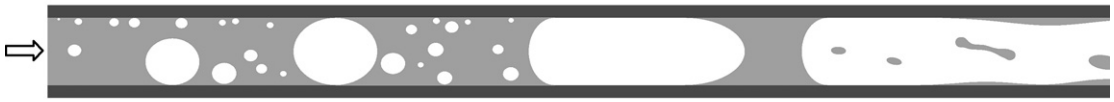

(b) Sketch of steady flow boiling pattern in microchannels with the Type-C connection

Fig. 12. Photos and sketch of steady flow boiling patterns in parallel microchannels ($D_h = 186$ μm) with the Type-C connection at $q = 364.68$ kW/m^2, $G = 124.03$ kg/m^2 s and $T_{in} = 35$ °C ($x_e = 0.359$).

Fig. 12(a) presents the photos showing the steady flow boiling patterns in four different locations in the microchannels with the Type-C connection at $q = 364.7$ kW/m^2, $G = 124$ kg/m^2 s and $T_{in} = 35$ °C (i.e., $x_e = 0.359$). It can be seen that isolated bubbles detached near the entrance (i) and moved downstream. As a result of bubble coalescence shown in (ii), vapor plugs were formed in (iii). Near the outlet (iv) the boiling pattern was annular flow with some water droplets formed on the bottom surface of the top Pyrex cover. The corresponding steady flow boiling patterns in the microchannels are sketched in Fig. 12(b), where the flow pattern near the entrance was similar to the steady bubbly/slug flow shown in Fig. 6(b). It appears from Fig. 12(b) that Taylor bubbles are the characteristic boiling flow pattern in microchannels.

Fig. 13 shows that thin film nucleation, such as that discussed by Balasubramanian and Kandlikar [21], indeed occurred occasionally in the thin liquid film at certain locations in the corner of a microchannel near the outlet. It can be seen that these bubbles had a flattened shape with a small contact angle as compared with a single bubble nucleation in a subcooled liquid flow (see Fig. 6(a)(i)). In addition, the nucleation lifetime in the thin liquid film was rather short (about 0.14 ms) compared to that of a nucleated bubble in a subcooled liquid (about 10–30 ms). Thus, the heat transfer mechanism in both the vapor plug and annular flow was a combination of liquid film vaporization and nucleate boiling.

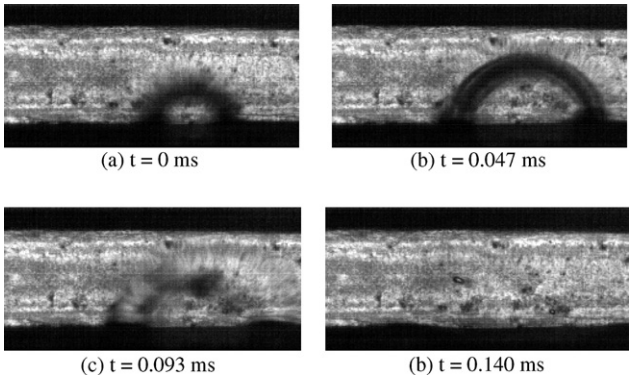

Fig. 13. Photos of nucleation in the thin film of annular flow near outlet section in parallel microchannels ($D_h = 186$ μm) at $q = 364.68$ kW/m^2, $G = 124.03$ kg/m^2 s and $T_{in} = 35$ °C ($x_e = 0.359$).

Fig. 14 presents photos for flow boiling patterns at $q = 364.7$ kW/m^2 and at three higher (compared with Fig. 12) mass fluxes near the outlet section of the microchannels. Since no reversed flow of vapor bubbles was observed in parallel microchannels with the Type-C connection, temperature and pressure were constant with time (i.e., a steady flow). Fig. 14(a) shows that flow boiling exhibited nucleate boiling characteristics with small isolated bubbles at a negative local vapor quality ($x_e = -0.034$). Fig. 14(b) shows that when the local vapor quality was nearly equal to zero ($x_e = 0.005$), the bubbles filled the entire cross-section and then were flushed out of the channels. This resulted in the maximum value of heat transfer coefficient, as discussed below. Fig. 14(c) shows that at an exit vapor quality of $x_e = 0.26$, local dryout was observed instantaneously from $t = 24.6$–65.9 ms, and the lifetime of the dryout increased with the increasing vapor quality. It can be speculated that the liquid film in the Taylor bubbles ruptures easily, causing dryout in microchannels.

3.3.2. Pressure drop characteristics in microchannels

Although steady flow boiling with no reversed flow of vapor bubble can be achieved by fabrication of inlet restriction (i.e., with the Type-C connection), this increase in flow stability came at the expense of higher pressure drop as can be seen by comparing the pressure drop in Fig. 15(a) and (b) for the Type-B and Type-C connections, respectively. For example, consider the pressure drop at the onset of flow instability (OFI), which was at the minimum point of the pressure-drop-versus-mass-flux curve. At this point,

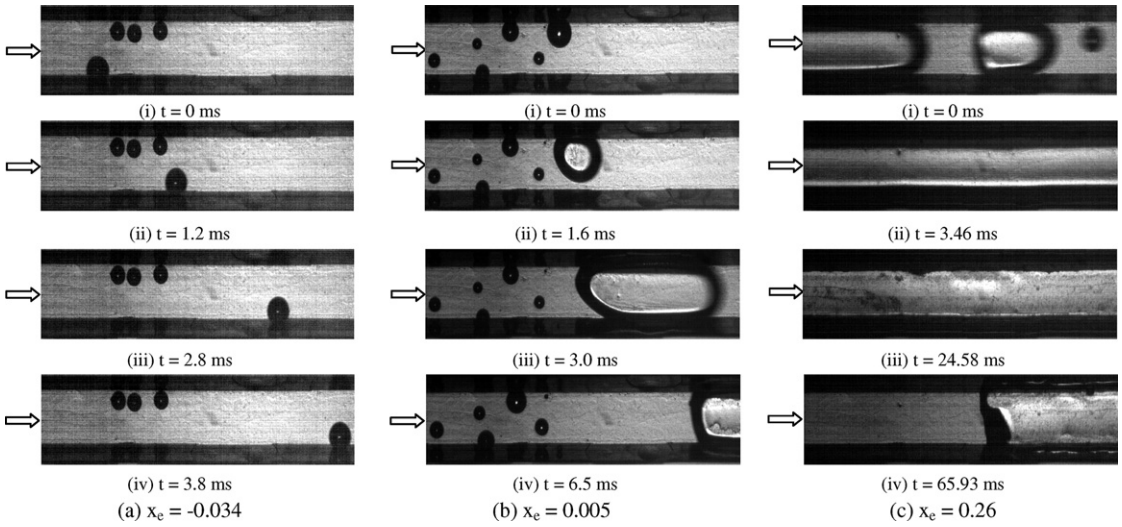

Fig. 14. Photos of steady flow boiling patterns near outlet section of parallel microchannels ($D_h = 186$ μm) with the Type-C connection at $q = 364.68$ kW/m^2 and $T_{in} = 35$ °C: (a) $G = 682.11$ kg/m^2 s (i.e., $x_e = -0.034$), $h_{local} = 14.834$ kW/m^2 K; (b) $G = 471.32$ kg/m^2 s (i.e., $x_e = 0.005$), $h_{local} = 29.428$ kW/m^2 K, (c) $G = 156.04$ kg/m^2 s (i.e., $x_e = 0.26$), $h_{local} = 12.12$ kW/m^2 K.

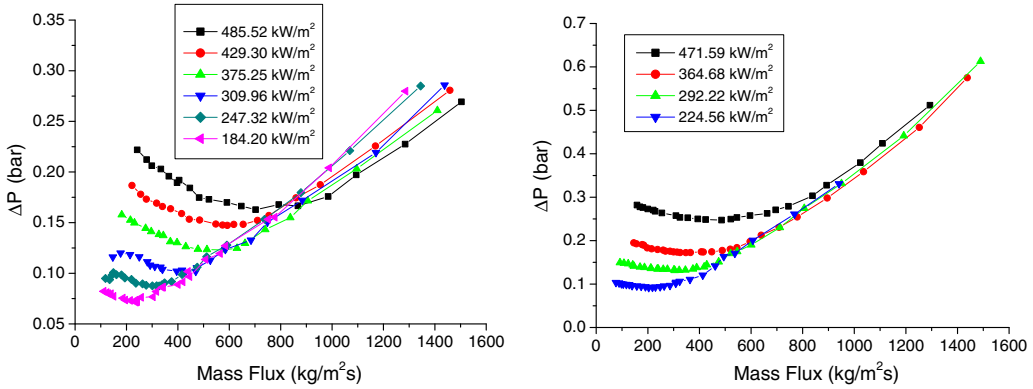

(a) Type-B connection (b) Type-C connection

Fig. 15. Measurements of inlet pressure versus mass flux in parallel microchannels ($D_h = 186$ μm) with (a) Type-B and (b) Type-C connections.

the pressure drop in microchannels with the Type-C connection for $q = 364.7$ kW/m^2 (see Fig. 15b) was 0.1723 bar, which is higher than 0.1231 bar for $q = 375$ kW/m^2 (see Fig. 15a) with the Type-B connection. The difference, of course, was the pressure drop due to the inlet restriction. Furthermore, it is possible to operate below the minimum without incurring the excursive instability for the Type-B connection. However, the oscillations do occur, and at higher heat flux would become violent enough to cause burnout [17,18]. Pressure drop data for flow boiling in microchannels with the Type-B and Type-A connections were obtained by Xu et al. [22] and by Wu et al. [23] previously. The difference between a macrochannel and a microchannel is that it is possible to operate in the negative sloping portion of the pressure-drop-versus-flow-rate curve with microchannels because the considerable fluctuations are not catastrophic, although it is not possible to go very far up the negative sloping portion of the pressure drop without encountering large scale dryout.

The pressure drop data in Fig. 15(a) and (b) are replotted in Fig. 16(a) and (b) in terms of pressure drop versus exit vapor quality. Fig. 16(a) shows that the OFI occurred at $x_e = -0.003$ (corresponding to $q/G = 0.722$ kJ/kg and inlet water temperature of 35 °C) in the Type-B connection and Fig. 16(b) shows that OFI occurred at $x_e = 0.046$ (corresponding to $q/G = 1.022$ kJ/kg and inlet water temperature of 35 °C) in the Type-C connection. This shows that inlet restriction had a significant effect on the values of local vapor quality at the OFI.

The total pressure drop between the inlet plenum and outlet plenum of the microchannels can be expressed as [14]

$$\Delta P = \Delta P_c + \Delta P_{re} + \Delta P_{sp} + \Delta P_{tp} + \Delta P_e \quad (4)$$

where ΔP_c is the inlet contraction pressure loss; ΔP_{re} is the pressure drop in the inlet restriction; ΔP_e is the outlet expansion pressure loss; ΔP_{sp} is the pressure drop in the single-phase flow region, and ΔP_{tp} is the two-phase pressure drop in the microchannel. Computations of all

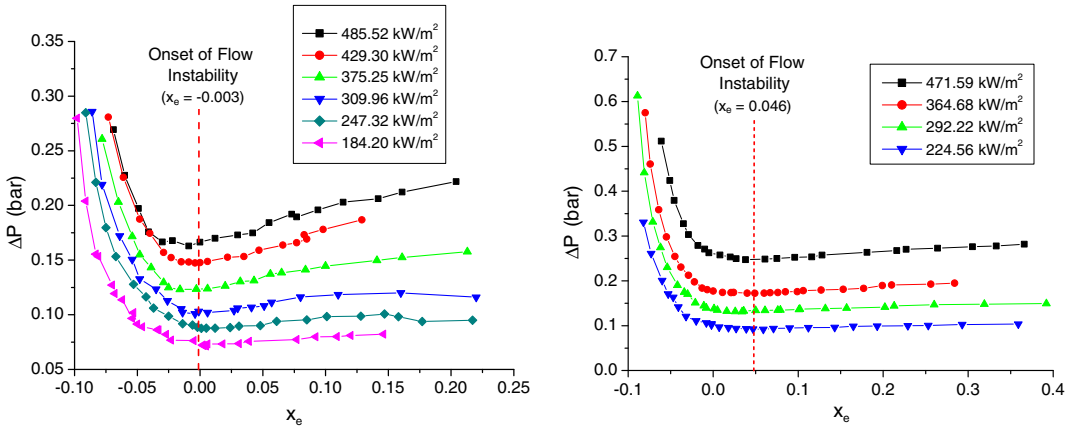

(a) Type-B connection (b) Type-C connection

Fig. 16. Measurements of inlet pressure versus local vapor quality in parallel microchannels ($D_h = 186$ μm) with the Type-B and Type-C connections at different heat fluxes.

components of ΔP in Eq. (4) except ΔP_{tp} were fairly straightforward, which had been discussed by Qu and Mudawar [14]. In the following paragraph, ΔP_{tp} obtained from the present experiment will be compared with Mishima and Hibiki's correlation [24] and Qu and Mudawar's correlation [14], which is a modification of Mishima and Hibiki's correlation by incorporating a mass flux term in the Martinelli–Chisholm constant C.

Fig. 17 is a comparison of four sets of pressure drop data for various heat fluxes (taken from Fig. 16b) with Mishima and Hibiki's correlation [24] for two-phase pressure drop. It can be seen that the correlation predicted the general trend of pressure drop, but underpredicted the present pressure drop data, especially at high vapor quality ($x_e > 0.1$). The reason that correlations for macrochannel fail to predict the pressure drop in microchannel may be attributed to different flow behavior in microchannels. The coalesced bubbles (in Fig. 12(a)(ii)) were confined, elongated (in Fig. 12(a)(iii)) and finally formed annular flow (in Fig. 12(a)(iv)) downstream. While in a macrochannel, many bubbles grew and flowed along the channel without restriction. Also, local dryout occurred at high vapor quality that caused vapor blocking the channels. Thus, the greater pressure drop in microchannels resulted from additional friction related to the elongated bubbles [25] as well as local dryout.

Fig. 18 is a plot of $\Delta P_{pred}/\Delta P_{exp}$ and the mean absolute error (MAE) versus exit vapor quality for the four sets of experimental data. The mean absolute error is defined as

$$\mathrm{MAE} = \frac{1}{M}\sum \frac{|\Delta P_{exp} - \Delta P_{pred}|}{\Delta P_{exp}} \times 100\%$$

where M is the number of data points. From this figure, it is shown that Mishima and Hibiki's correlation [24] underpredicted the pressure drop data with a MAE of 22.7%. Compared with the present pressure drop data, Qu and Mudawar's correlation [14] with the MAE of 20.2% is slightly better than Mishima and Hibiki correlation [24], which is not presented here.

3.3.3. Boiling heat transfer coefficient in microchannels

Fig. 19 shows the dependence of the flow boiling heat transfer coefficient on the local vapor quality near the

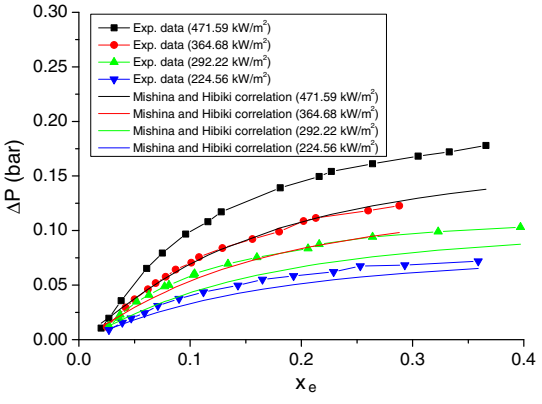

Fig. 17. Comparison of pressure drop data with Mishima and Hibiki correlation for flow boiling in mini/micochannel ($D_h = 186$ μm) at different heat fluxes.

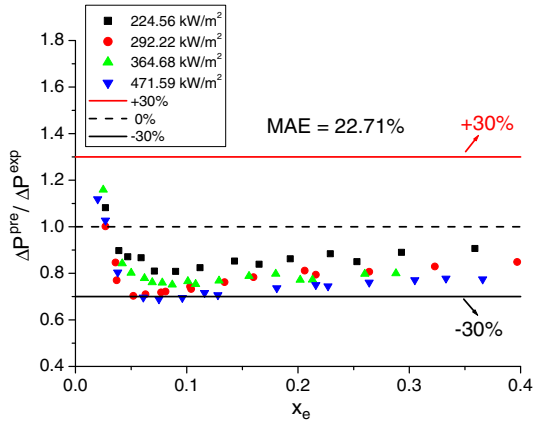

Fig. 18. Pressure drop ratio versus vapor quality in parallel microchannels ($D_h = 186$ μm) at different heat fluxes.

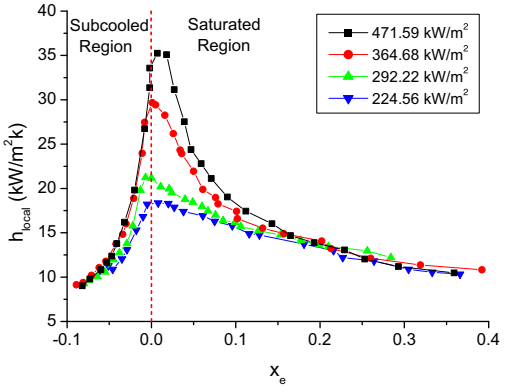

Fig. 19. Boiling heat transfer coefficient versus local vapor quality near outlet section in parallel microchannels ($D_h = 186$ μm) with the Type-C connection at different heat fluxes.

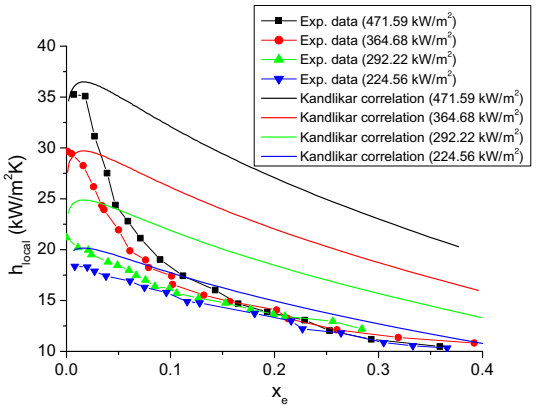

Fig. 20. Comparison of boiling heat transfer coefficient data with Kandlikar correlation for flow boiling in macrochannels ($D_h = 186$ μm) at different heat fluxes.

outlet section (T_{w5}) in microchannels at the exit pressure with the Type-C connection. The range of the measured heat transfer coefficient, h_{local} at the exit from this experiment varied from 9 to 35 kW/m^2 K, which was similar to the values of 10–30 kW/m^2 K measured by Hetsroni et al. [11] and the values of 10–25 kW/m^2 K measured by Chen and Garimella [20]. However, our measurements were smaller than the values of 20–45 kW/m^2 K measured by Qu and Mudawar [26].

It is shown from Fig. 19 that the heat transfer coefficient increased with the increase of vapor quality in the subcooled boiling region ($x_e < 0$) due to a transition from partial to fully developed nucleate boiling. The trend of decreasing heat transfer coefficient with increasing vapor quality in the saturated boiling region of $x_e > 0$ was similar to those measured by Hetsroni et al. [11], as well as by Qu and Mudawar [26]. However, this trend was contradictory to those by Chen and Garimella [20], who found that the heat transfer coefficient increased with local vapor quality in the region of $x_e > 0$ and then decreased at higher vapor quality. Moreover, it is shown from Fig. 19 that the heat transfer coefficient increased with the increase of heat flux at low vapor quality ($x_e < 0.2$). But at higher vapor qualities, the heat transfer coefficient was independent of heat flux, which was caused by dryout.

Kandlikar's correlation equation [27] for flow boiling heat transfer in large diameter tubes (with an inner diameter large than 3 mm) has been used in previous studies [26,28,29] to correlate microchannel and minichannel heat transfer data with moderate agreement. Fig. 20 is a comparison of the Kandlikar correlation with the present experimental data for $x_e > 0$ (taken from Fig. 19). It is shown that although the correlation predicted the general trend of the present boiling heat transfer coefficient data, it overpredicted the data in high heat flux and high vapor quality regimes. This can be attributed to the occurrence of local dryout (Fig. 14(c)(iii)) under high heat flux and high vapor quality conditions. Fig. 21 is a plot of $h_{local,Kandikar}/h_{local,exp}$ and the mean average error (MAE) of heat transfer coefficient versus local vapor quality, where

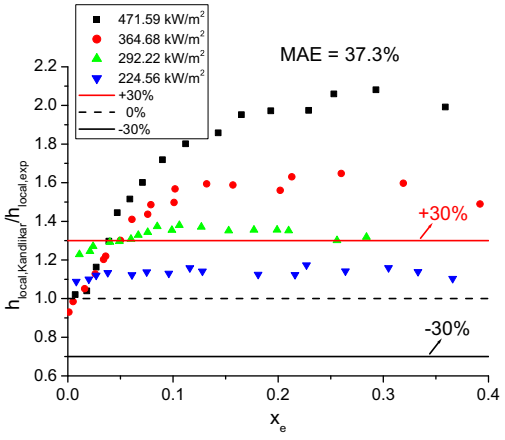

Fig. 21. Heat transfer coefficient ratio versus vapor quality in parallel microchannels ($D_h = 186$ μm) at different heat fluxes.

$$\mathrm{MAE} = \frac{1}{M}\sum \frac{|h_{local,exp} - h_{local,pred}|}{h_{local,exp}} \times 100\%$$

It is shown that Kandlikar's correlation [27] for flow boiling in macrochannels overpredicted the present data for flow boiling in microchannels with a MAE of 37.3%.

4. Concluding remarks

In this paper, flow boiling instability in parallel microchannels with three types of inlet/outlet connections (shown as Type-A, Type-B and Type-C connections in Fig. 3) have been investigated experimentally. The following conclusions can be drawn from the present work:

1. For flow boiling in microchannels without inlet restrictions (i.e., Type-A and Type-B connections), temperature and pressure oscillations occur when a bubble grows to touch the confining wall and expands upstream.
2. For flow boiling in microchannels with the Type-A and Type-B connections where reversed flow of vapor

occurred, the exit vapor quality can be used to classify the steady and unsteady flow boiling regimes.

3. The configuration between the inlet and outlet plenums with the microchannels greatly affected the amplitude of flow-boiling instabilities. This is the reason why different investigators found different amplitudes of temperature and pressure oscillations under similar mass flux and heat flux conditions. In microchannels with the Type-A connection where the outlet conduit was perpendicular to the microchannels, the amplitudes of pressure and temperature fluctuations and the strength of the reversed vapor flow were the highest among the three types of connections because the outlet configuration is most restrictive.
4. For microchannels with the Type-C connection where flow entering to the microchannels is restricted, steady flow boiling with no oscillations of temperature and pressure can be achieved. In these microchannels, no reversed flow of vapor bubbles was observed under the experimental conditions. This configuration is recommended for high-heat-flux microchannel applications to avoid large temperature fluctuations and early burnout. Future work should be directed toward assessing the amount of inlet throttling (pressure drop penalty) required for stabilization.
5. In vapor plugs and annular flow, nucleation in the thin liquid film was occasionally observed at certain locations in the corner of a microchannel. The nucleation life-time in the thin liquid film was rather short (about 0.14 ms) compared to bubble nucleation in a subcooled liquid (about 10–30 ms). Thus, the heat transfer mechanism in the vapor plug and annular flow was the combination of liquid film vaporization and nucleate boiling.
6. Although Qu and Mudawar's correlation is slightly better than Mishima and Hibiki's correlation in predicting pressure drop in microchannels obtained from the present experiment, both correlations underpredict the pressure data at high vapor quality, probably due to different flow behavior in microchannels.
7. Heat transfer coefficients have been obtained for flow boiling microchannels with the Type-C connection. It is found that the heat transfer coefficient at the exit increases with the increase of the exit vapor quality in the subcooled boiling region ($x_e < 0$) due to a transition from partial to fully developed nucleate boiling. On the other hand, the heat transfer coefficient at the exit decreases with the increase of the exit vapor quality in the saturated boiling region ($x_e > 0$) due to the presence of local dryout.
8. The heat transfer coefficient data in low heat flux or low vapor quality in saturated flow boiling in microchannel agrees well with the correlation developed by Kandlikar [27] for flow boiling in macrochannels. However, boiling heat transfer coefficient data at high heat flux and high vapor quality are lower than those predicted by Kandlikar correlation, probably due to the occurrence of local dryout.

Acknowledgements

This work was supported by the National Natural Science Foundation of China through Grant No. 50536010 and by Shanghai Municipal Science and Technology Committee through Grant No. 05JC14025.

References

[1] J.A. Boure, A.E. Bergles, L.S. Tong, Review of two-phase flow instability, Nucl. Eng. Des. 25 (1973) 165–192.
[2] R.S. Daleas, A.E. Bergles, Effect of upstream compressibility on subcooled critical heat flux. ASME Paper No. 65-HT 67, ASME, New York.
[3] A.E. Bergles, Burnout in boiling heat transfer. Part III: High-quality forced-convection systems, Accident Anal. 20 (1979) 671–689.
[4] P. Cheng, H.Y. Wu, Mesoscale and microscale phase-change heat transfer, Adv. Heat Transfer 39 (2006) 461–573.
[5] P. Cheng, H.Y. Wu, F.J. Hong, Phase-change heat transfer in microsystems, J. Heat Transfer 129 (2007) 101–108.
[6] D. Brutin, F. Topin, L. Tadrist, Experimental study of unsteady convective boiling in heated minichannels, Int. J. Heat Mass Transfer 46 (2003) 2957–2965.
[7] G. Hetsroni, A. Mosyak, Z. Segal, G. Ziskind, A uniform temperature heat sink for cooling of electronic devices, Int. J. Heat Mass Transfer 45 (2002) 3275–3286.
[8] G. Hetsroni, A. Mosyak, Z. Segal, Nonuniform temperature distribution in electronic devices cooled by flow in parallel microchannels, IEEE Trans. Component Packing Technol. 24 (2001) 17–23.
[9] H.Y. Wu, P. Cheng, Visualization and measurements of periodic boiling in silicon microchannels, Int. J. Heat Mass Transfer 46 (2003) 2603–2614.
[10] H.Y. Wu, P. Cheng, Boiling instability in parallel silicon microchannels at different heat flux, Int. J. Heat Mass Transfer 47 (2004) 3631–3641.
[11] G. Hetsroni, A. Mosyak, E. Pogrebnyak, Z. Segal, Explosive boiling of water in parallel micro-channels, Int. J. Multiphase Flow 31 (2005) 371–392.
[12] J.L. Xu, S. Shen, Y.H. Gan, Y.X. Li, W. Zhang, Q.C. Su, Transient flow pattern based microscale boiling heat transfer mechanisms, J. Micromech. Microeng. 15 (2005) 1344–1361.
[13] G.D. Wang, P. Cheng, H.Y. Wu, Unstable and stable flow boiling in parallel microchannels and in a single microchannel, Int. J. Heat Mass Transfer 50 (2007) 4297–4310.
[14] W.L. Qu, I. Mudawar, Measurement and prediction of pressure drop in two-phase micro-channel heat sinks, Int. J. Heat Mass Transfer 46 (2003) 2737–2753.
[15] S.G. Kandlikar, D.A. Willistern, J. Borrelli, Experimental evaluation of pressure drop elements and fabricated nucleation sites for stabilizing flow boiling in minichannels and microchannels, in: Proceedings of ASME 3rd International Conference on Microchannels and Minichannels, ICMM2005-75197, Toronto, Ontario, Canada, 2005.
[16] A.E. Bergles, J.H. Lienhard V, G.E. Kendell, P. Griffith, Boiling and evaporation in small diameter channels, Heat Transfer Eng. 24 (2003) 18–40.
[17] A.E. Bergles, S.G. Kandlikar, On the nature of critical heat flux in microchannels, J. Heat Transfer 127 (2005) 101–107.
[18] W.L. Qu, I. Mudawar, Measurement and correlation of critical heat flux in two-phase microchannel heat sinks, Int. J. Heat Mass Transfer 47 (2004) 2045–2059.
[19] A. Kosar, C.J. Kuo, Y. Peles, Suppression of boiling flow oscillations in parallel microchannels by inlet restrictors, J. Heat Transfer 128 (2006) 251–260.

[20] T. Chen, S.V. Garimella, Measurements and high-speed visualizations of flow boiling of a dielectric fluid in a silicon microchannel heat sink, Int. J. Multiphase Flow 32 (2006) 957–971.
[21] P. Balasubramanian, S.G. Kandlikar, Experimental study of flow patterns, pressure drop, and flow instabilities in parallel rectangular minichannels, Heat Transfer 26 (2005) 20–27.
[22] J.L. Xu, J.J. Zhou, Y.H. Gan, Static and dynamic flow instability of a parallel microchannel heat sink at high heat flux, Energy Convers. Manage. 46 (2005) 313–334.
[23] H.Y. Wu, P. Cheng, H. Wang, Pressure drop and flow boiling instabilities in silicon microchannel heat sinks, J. Micromech. Microeng. 16 (2006) 2138–2146.
[24] K. Mishima, T. Hibiki, Some characteristics of air–water two-phase flow in small diameter vertical tubes, Int. J. Multiphase Flow 22 (1996) 703–712.
[25] T.Y. Tran, M.C. Chyu, M.W. Wambsganss, D.M. France, Two-phase pressure drop of refrigerants during flow boiling in small channels: an experimental investigation and correlation development, Int. J. Multiphase Flow 26 (2002) 1739–1754.
[26] W.L. Qu, I. Mudawar, Flow boiling heat transfer in two-phase micro-channel heat sinks – I. Experimental investigation and assessment of correlation methods, Int. J. Heat Mass Transfer 46 (2003) 2755–2771.
[27] S.G. Kandlikar, A general correlation for saturated two-phase boiling heat transfer inside horizontal and vertical tubes, J. Heat Transfer 112 (1990) 219–228.
[28] S.G. Kandlikar, An extension of the flow boiling correlation to transition, laminar, and deep laminar flows in minichannels and microchannels, Heat Transfer Eng. 25 (2004) 86–93.
[29] S.G. Kandlikar, Fundamental issues related to flow boiling in minichannels and microchannels, Exp. Therm. Fluid Sci. 26 (2002) 389–407.